CdTe Detector Data and Data Reduction for Calibration of ART Mirror Modules

Prepared by: Douglas A. Swartz

NASA, Marshall Space Flight Center

December 4, 2018

Abstract

This document describes the reduction of data obtained with a CdTe detector for the calibration of the ART mirror modules at MSFC's Stray Light Facility and the content and format of the data. This report also provides the effective area and half-power diameter (with uncertainties) of each mirror module as smooth (differentiable) functions of off-axis angle at a pre-defined set of 13 energy groups spanning 4 to 30 keV.

Revision History

Revision	Author	Date	Change
v1.0	DAS/USRA	07/11/2014	Initial Release
v2.0	DAS/USRA	29/11/2018	convert to template

Contents

List of Figures

List of Tables

1 Experimental Setup

Details of the experimental setup are documented in the ART-XC Mirror Modules Calibration Plan (CP) v.7. Only measurements involving the Amptek XR-100T CdTe detector are considered in this report. The active area (field of view) of the detector is a 5.115×5.115 mm square but this can be reduced, depending on the experiment, using any of a series of circular apertures (pinholes) as tabulated in Figure 1. The detector can be placed, relative to the facility optical axis and the location of the mirror module along that axis, using a 3-axis translation stage. The plane perpendicular to the optical axis is referred to herein as the (x, y) plane and the optical axis as the z-axis. The schematic in Figure 1 shows the square detector active area, the relative area of the various pinholes, and the relative location of the detector in the (x, y) plane when using the 0.475 mm pinhole to perform the 7×7 point spread function (PSF) measurements.

In addition, the mirror module can be aligned relative to the optical axis using tip/tilt and pan/yaw stages to measure performance at off-axis angles, θ, along azimuthal directions, ϕ. As has been shown elsewhere,[1] the ART mirror modules are very nearly azimuthally-symmetric. Therefore, quantities measured along different azimuths are typically averaged for brevity.

In most measurements, the detector is placed in a "defocused" position 7 mm from the focal plane in the $+z$ direction towards the mirror module. A focal length of 2770 mm is assumed; the plate scale is therefore 1 mm = 1.24′ at the focus position.

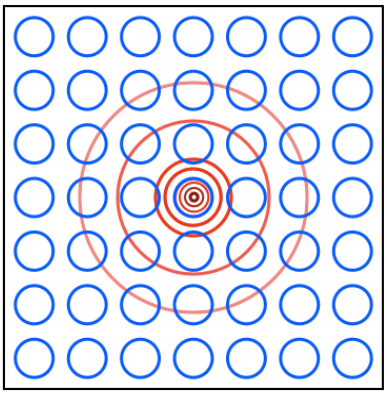

mm	sec
0.100	7.4
0.235	17.5
0.380	28.3
0.475	35.3
0.745	55.4
1.000	74.4
2.000	149.0
3.000	223.0

Figure 1: Schematic of the (x, y) plane perpendicular to the optical axis showing the full 5.115×5.115 mm^2 square active area of the CdTe detector, the relative sizes of each of the 8 pinholes, and the placement (and 0.475 mm aperture) used for the 7×7 0.7 mm-step point spread function scans. The table lists the pinhole sizes in mm and arcseconds.

2 File Formats and Naming Conventions

All data files are comma-separated value (csv) plain text files containing 520 fields (columns) and from 1 to 49 records (rows). The first 8 fields are (1) a Microsoft-encoded record creation date/time, (2) detector horizontal and (3) vertical offset from the optical axis, (4) requested exposure time, (5) actual exposure time, (6) deadtime-corrected exposure time, (7) detector high voltage reading, and (8) unused (always =0). The remaining 512 fields contain the count spectrum, C_i, $(i = 1, 512)$ obtained over the exposure time.[2] Unit of time is seconds and of length is mm.

Files are named, in part, by the operator and in part by the software driving the various stages and controlling the detector. The naming convention attempts to summarize the experimental setup and thus includes X-ray source power settings (voltage and current), detector aperture settings (pinhole diameter), mirror module orientation (θ and ϕ), and measurement type (EA, HPD, or PSF; see below). In addition, the module identification, detector system (CdTe), measurement type, and detector location relative to

[1] e.g., Gubarev et al. 2014

[2] In rare instances, the requested and actual exposure times differ by $\gg 10\%$ indicating an error has occurred in which the current record is the sum of data from the current exposure plus the previous exposure plus any "slew" time needed to reposition either the detector or the mirror module or both. In these cases, the previous exposure record is subtracted from the current exposure record and a revised record (with the actual time and count spectrum updated) is written into the file. This process is performed post-facto.

the aimpoint is documented in the directory pathname to each data file. For practical purposes, file and path (directory) names containing blank spaces are replaced with underscores. An example of a filename is ARTM1_EA_nopin_focus-7mm_15kV_0.02mA_45deg_-9arcmin_20140804-120020.csv denoting an effective area (EA) measurement of mirror module 1 (M1) set at the standard defocus position (focus-7mm), azimuthal angle ϕ=45° (45deg) and offset angle θ=-9′ (-9arcmin), and using a source voltage setting of 15 kV (15kV) and current of 0.02 mA (0.02mA). The file was first written to on the given local date and time (20140804-120020).

The channel to energy conversion for the spectrum is $E_i = 0.1073i - 0.470$ keV, $i = 1, 512$. Energy-dependent quantities are reported for 13 energy groups, E_g, as listed in Table 1 along with their channel boundaries.

Table 1: Energy Bands E_g & Corresponding Channel Ranges

Energy (keV)	$4-5$	$5-6$	$6-7$	$7-8$	$8-9$	$9-10$	$10-12$
Channel	$42-50$	$51-60$	$61-69$	$70-78$	$79-88$	$89-97$	$98-116$
Energy (keV)	$12-14$	$14-16$	$16-18$	$18-20$	$20-25$	$25-30$	
Channel	$117-134$	$135-153$	$154-172$	$173-190$	$191-237$	$238-283$	

3 Effective Area

The effective area (EA) of a mirror module at energy channel E_i and off-axis angle θ is

$$EA(E_i, \theta) = \frac{A_s}{1.052597} \left[\frac{C(E_i, \theta)}{B(E_i, \theta)} \right] \tag{1}$$

where A_s is the detector aperture area when no mirror module is in the optical path, $B(E_i, \theta)$ is the observed count rate for this configuration, $C(E_i, \theta)$ is the count rate with the mirror module in place and an infinite area aperture, and the numerical constant accounts for the additional distance of the detector from the entrance to the mirror module. Count rates are derived from the count spectra and deadtime-corrected exposure times; e.g., $C(E_i, \theta) = C_i/t$ where t is the exposure time. In order to cover the entire energy range, $4.0 < E < 30.0$ keV, with good counting statistics but without introducing pileup of the strong Cu Kα line at $\sim 2E_l \sim 16$ keV, two independent EA measurements were made using two different X-ray source settings to adequately cover the low ($4 < E < 14$ keV) and high ($14 < E < 30$ keV) energy ranges.

The EA measurement uses a 3 mm diameter aperture providing an area of $A_s = 0.070686$ cm^2 in the "no optic" configuration. With the mirror module in the optical path, the full 26.163 mm^2 open area of the detector captures roughly 95% of the total flux focused by the mirror modules onto the detector plane at the standard $\Delta z = -7$ mm defocus position. A correction factor to account for this finite aperture is determined by performing a 5×5 (x, y) scan with the full detector aperture and a 5 mm step size at $\theta \equiv 0'$. The central 3×3 subset of this scan captures 100% of the focused flux. This correction factor has only been measured on-axis and for the standard defocused measurements. There are insufficient statistics to determine a detailed energy-dependent correction factor but correction factors have been computed on the appropriate energy ranges for each of the two X-ray source configurations used in the EA measurements. Table 2 lists these measured correction factors.

In order to characterize the off-axis dependence of the EA, measurements are made at a series of 17 off-axis angles, $-18' \leq \theta_j \leq 18'$, along each of four azimuthal angles, ϕ_k (k = 0°, 45°, 90°, 135°), as documented in the CP. This provides the equivalent of 8 off-axis measurements, θ, in eight azimuths, ϕ (plus a 4-times-sampled on-axis measurement). The effective areas, $EA(E_i, \theta_j)$, are then averaged over each of the 13 energy groups, E_g, listed in Table 1. The azimuthal symmetry was confirmed at each off-axis angle for each energy group and for each module by comparing $EA(E_g, \theta_j)$ as a function of ϕ to a constant.

Table 2: Finite Aperture Effective Area Correction Factors

Module	1	2	3	4	5	6	7	8
low-E	1.0465	1.0447	1.0485	1.0495	1.0659	1.0542	1.0573	1.0567
high-E	1.0429	1.0457	1.0491	1.0531	1.0633	1.0536	1.0545	1.0604

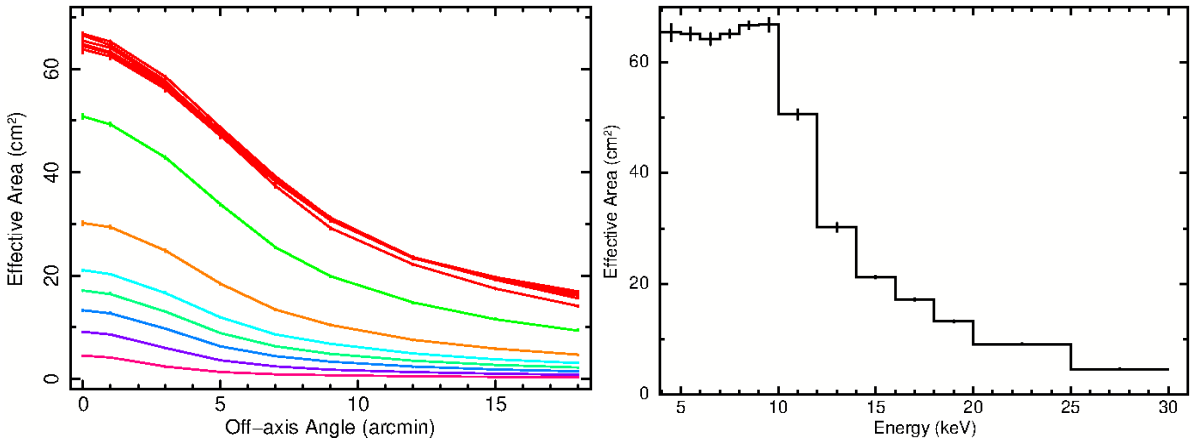

Figure 2: *Left:* The measured effective area is shown against off-axis angle, θ, for 13 energy groups, E_g, for mirror Module 1. The EA has been averaged over the 8 measurement azimuths. The topmost 6 curves are displayed in the same color to emphasize their similarity. They correspond to the 6 lowest energy groups spanning 4 to 10 keV. The effective area decreases monotonically with increasing energy at higher energies. *Right:* On-axis effective area (at $\theta \equiv 0$)) is shown against X-ray energy for mirror Module 1. Data is shown for azimuthal angle $\phi = 0\,\mathrm{deg}$. Errors are purely statistical. No aperture correction has been applied. The EA at and below energy group $g = 8$ (12−14 keV) is computed using the low-energy source setting measurements and the EA at higher energies is computed using the high-energy setting measurements.

The measured EA, with errors, as a function of θ is shown for each energy group for mirror Module 1 in Figure 2. The finite-aperture correction factors (Table 2) have *not* been applied. As can be seen, the EA is roughly independent of energy for energies $E \lesssim 10$ keV then declines monotonically for higher energies. This is also evident from the right side panel of Figure 2 which shows the on-axis EA for all energy groups for Module 1.

An empirical analytic function, the sum of two Gaussians,

$$EA_E(\theta) = A_1 e^{-(\theta-\theta_c)^2/2\sigma_1^2} + A_2 e^{-(\theta-\theta_c)^2/2\sigma_2^2}, \tag{2}$$

was fit to the distribution of EA with angle (averaged over ϕ; i.e., Figure 2 left panel) for each of the 13 energy groups E_g. The resulting best-fit parameter values and uncertainties are provided in Table 3 for each of the eight mirror modules. Here, the Gaussian norms, A, have been multiplied by the correction factors of Table 2.

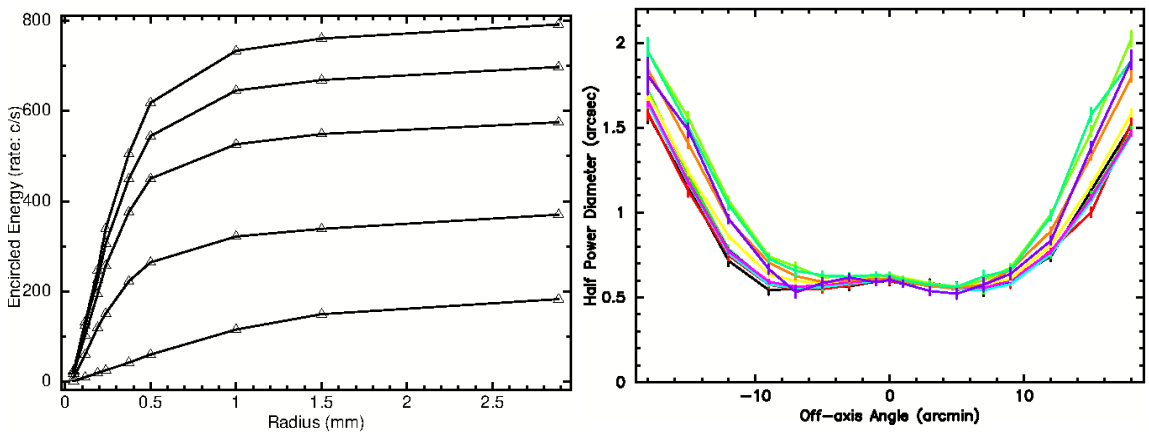

Figure 3: *Left:* Encircled energy at several off-axis angles is shown against radius for the energy group $8 < E < 9$ keV. Shown, from top to bottom, are the data for off-axis angles $\theta = 0$, 3, 5, 9, and 18 arcminutes for $\phi = 0$ deg for Module 6. Markers are used to better display individual data points because the (statistical) error bars are small. Units on the ordinate are counts $\sec^{-1}$. *Right:* Half-power diameter, $HPD_E(\theta)$, for the 13 energy groups for Module 6. The characteristic shape of the distribution over off-axis angle, θ, is due to the "defocus" location of the detector. At focus, the curve would be roughly parabolic and centered near $\theta = 0$.

These quantities can be used to estimate the EA over the continuous range of off-axis angles $0'$ to $18'$ and azimuths $0°-360°$ for any energy group, E_g. Note that the peak of the Gaussian functions occurs at unphysical values $\theta_c \leq 0$. This is because the EA is more strongly peaked than a Gaussian function near its centroid.

For comparison, the on-axis *measured* EA values (averaged over the four azimuthal measurements) is provided in Table 4. Again, the correction factors of Table 2 have been applied.

4 Half Power Diameter

The half-power diameter of a mirror module is derived from encircled energy measurements which are proportional to the focussed flux passing through an aperture aligned perpendicular to the optical axis. The left panel of Figure 3 displays the encircled energy curves at several off-axis angles for the X-ray energy group $8 < E < 9$ keV. Similar curves have been constructed for a series of off-axis angles, θ_j, measured along each of two azimuthal directions, ϕ_k ($k = 0°$, $90°$), and at all energy groups for each mirror module. These curves have been fit to functions of the form:

$$h_E(r) = A\left(1 - (2(r - r_c)/\sigma_L)^{-2}\right) \tag{3}$$

where r is the encircled energy radius and the dependence on θ and incident energy, E, has been suppressed for clarity. This function is the sum of a constant and a Lorentzian centered at r_c with FWHM σ_L. The half-power radius, $r_{1/2}$ is obtained by analytical integration of this function, $\int_0^{r_{1/2}} h_E(r)dr$, setting it equal to $(1/2)\int_0^{R_{\max}} h_E(r)dr$, and solving for $r_{1/2}$. Here $R_{\max} \equiv 2.886$ mm corresponds to the encircled energy radius equivalent to the full detector open area and it is assumed that $R_{\max}$ encircles 100% of the focussed energy. Thus, $r_{1/2}$ and its uncertainty can be expressed as analytical functions of r_c and σ_L and their uncertainties. The result is then converted to a HPD in angular units. The resulting derived HPD is shown as a function of θ for one mirror module in the right-hand panel of Figure 3. Here, the HPD was averaged over azimuthal angle ϕ and is shown for each of the 13 energy groups, E_g. An empirical analytic function,

$$HPD_E(\theta) = A_1 e^{-(\theta-\theta_1)^2/\sigma_1^2)} + A_2 e^{-(\theta-\theta_2)^2/\sigma_2^2)} + A_3, \tag{4}$$

was fit to the distribution of HPD with off-axis angle, θ. The resulting best-fit parameter values and uncertainties are provided in Table 5 for each of the mirror modules tested.
These quantities can be used to estimate the HPD over the continuous range of off-axis angles 0° to 18° for any energy group E_g. For example, the central values, $HPD_E(\theta \equiv 0)$, and uncertainties (derived from Table 5) are listed in Table 6 for each module and each energy group.
Figure 4 displays the HPD against the off-axis angle, θ, for all mirror modules. These HPD curves have been averaged over the two azimuths, ϕ=0°, 90°.

5 Point Spread Function

The PSF of each mirror module was sampled using the CdTe detector with a 0.475 mm pinhole. The sampling used a 7×7-position scan with a 0.7 mm step size in the (x, y) plane as shown in Figure 1. The PSF was sampled in this way over a range of off-axis angles, θ, along two azimuthal directions, ϕ. A 7×7 "pixel" FITS image was constructed from each scan using the FTOOLS utility `flst2im` for display purposes. No formal analysis of the PSF measurements was undertaken.

Table 3: $EA_E(\theta)$ (Eq. 2) fit parameters

Energy (keV)	θ_c (arcmin)	σ_1 (arcmin)	A_1 (cm^2)	σ_2 (arcmin)	A_2 (cm^2)
Module 1					
4-5	-0.67±0.34	5.54±0.30	41.57±1.90	21.16±1.78	25.60±1.42
5-6	-0.55±0.25	5.47±0.22	42.01±1.40	21.04±1.32	25.94±1.06
6-7	-0.51±0.23	5.36±0.20	40.73±1.25	19.67±0.97	26.86±0.95
7-8	-0.47±0.14	5.18±0.12	39.90±0.75	17.84±0.43	28.76±0.56
8-9	-0.36±0.12	5.01±0.10	39.82±0.59	16.57±0.28	30.06±0.45
9-10	-0.36±0.22	4.83±0.18	39.99±1.07	15.55±0.44	29.49±0.79
10-12	-0.47±0.19	4.60±0.14	33.03±0.69	15.16±0.35	20.35±0.44
12-14	-0.54±0.25	4.31±0.17	20.94±0.58	14.41±0.42	11.07±0.32
14-16	-1.24±0.14	4.47±0.08	15.68±0.23	14.86±0.17	7.26±0.08
16-18	-1.34±0.13	4.32±0.07	13.57±0.20	14.79±0.16	5.29±0.05
18-20	-1.33±0.13	4.10±0.07	10.98±0.17	14.16±0.15	3.78±0.04
20-25	-1.32±0.09	3.70±0.04	8.05±0.09	13.57±0.09	2.19±0.01
25-30	-1.96±0.17	3.40±0.07	4.64±0.13	12.45±0.12	0.98±0.01
Module 2					
4-5	-0.49±0.31	5.26±0.27	42.51±1.71	19.52±1.25	27.93±1.27
5-6	-0.62±0.26	5.34±0.22	43.34±1.42	19.54±0.99	28.48±1.04
6-7	-0.65±0.24	5.30±0.20	41.23±1.28	18.88±0.83	27.85±0.92
7-8	-0.42±0.14	5.06±0.12	39.86±0.70	17.38±0.38	28.84±0.52
8-9	-0.44±0.12	5.02±0.10	39.57±0.59	16.66±0.29	29.21±0.44
9-10	-0.34±0.21	4.77±0.17	39.02±0.99	15.63±0.43	28.27±0.72
10-12	-0.26±0.16	4.33±0.12	31.67±0.58	14.48±0.27	20.71±0.38
12-14	-0.80±0.28	4.39±0.19	20.00±0.61	14.72±0.46	10.30±0.31
14-16	-1.19±0.14	4.48±0.08	14.36±0.21	14.88±0.18	6.75±0.08
16-18	-1.84±0.16	4.60±0.09	13.77±0.25	15.33±0.20	5.10±0.06
18-20	-1.52±0.14	4.18±0.07	11.22±0.19	14.68±0.17	3.68±0.04
20-25	-1.69±0.11	3.86±0.05	7.63±0.11	13.88±0.11	2.02±0.01
25-30	-3.65±0.31	4.17±0.11	5.32±0.27	14.41±0.23	0.82±0.01
Module 3					
4-5	-0.51±0.32	5.41±0.28	40.84±1.74	20.70±1.58	26.21±1.33
5-6	-0.44±0.23	5.43±0.21	39.97±1.27	21.29±1.32	25.05±0.99
6-7	-0.39±0.21	5.33±0.19	40.64±1.18	20.25±1.03	26.31±0.91
7-8	-0.36±0.13	5.14±0.12	38.91±0.69	18.08±0.44	27.94±0.53
8-9	-0.34±0.11	5.08±0.10	38.91±0.57	16.99±0.30	28.49±0.43
9-10	-0.15±0.19	4.74±0.16	36.99±0.87	15.57±0.41	27.41±0.67
10-12	-0.28±0.17	4.51±0.13	31.85±0.61	14.94±0.32	20.13±0.42
12-14	-0.60±0.26	4.37±0.18	20.49±0.59	14.45±0.44	11.00±0.33
14-16	-1.01±0.12	4.39±0.07	14.16±0.18	14.75±0.17	6.61±0.07
16-18	-1.26±0.13	4.31±0.07	12.32±0.17	14.72±0.16	4.84±0.05
18-20	-1.07±0.11	3.91±0.06	9.82±0.13	13.84±0.13	3.47±0.03
20-25	-1.79±0.10	3.88±0.05	7.54±0.10	14.10±0.10	1.84±0.01
25-30	-2.11±0.19	3.57±0.08	3.69±0.11	12.80±0.16	0.71±0.01
Module 4					
4-5	-0.29±0.27	5.28±0.24	40.10±1.45	21.74±1.67	24.81±1.13
5-6	-0.57±0.23	5.55±0.21	41.35±1.30	23.07±1.68	23.77±0.98
6-7	-0.46±0.21	5.39±0.19	41.88±1.17	21.78±1.26	25.12±0.89
7-8	-0.31±0.12	5.18±0.11	39.34±0.63	19.51±0.53	25.50±0.49
8-9	-0.32±0.10	5.17±0.09	40.32±0.56	18.61±0.40	26.31±0.43
9-10	-0.40±0.21	5.07±0.17	40.75±1.07	17.50±0.65	25.47±0.79
10-12	-0.29±0.16	4.59±0.12	32.29±0.58	15.91±0.38	18.50±0.39
12-14	-0.53±0.24	4.39±0.17	21.08±0.56	15.14±0.48	10.37±0.31
14-16	-1.02±0.12	4.45±0.07	15.06±0.20	15.32±0.19	6.57±0.07
16-18	-1.09±0.12	4.24±0.07	12.60±0.16	14.85±0.17	4.83±0.05
18-20	-1.37±0.13	4.09±0.07	10.23±0.16	14.57±0.16	3.36±0.03
20-25	-1.82±0.11	3.99±0.05	6.81±0.09	14.51±0.11	1.65±0.01
25-30	-4.65±0.45	4.55±0.15	4.88±0.36	14.91±0.34	0.63±0.01

Table 4: $EA_E(\theta)$ (Eq. 2) fit parameters *(cont.)*

Energy (keV)	θ_c (arcmin)	σ_1 (arcmin)	A_1 (cm^2)	σ_2 (arcmin)	A_2 (cm^2)
			Module 5		
4-5	-0.64±0.33	5.40±0.28	38.39±1.64	19.67±1.33	24.73±1.21
5-6	-0.69±0.26	5.43±0.22	39.58±1.32	19.90±1.07	25.11±0.97
6-7	-0.58±0.23	5.29±0.20	37.69±1.12	19.01±0.83	25.26±0.82
7-8	-0.51±0.14	5.11±0.12	36.95±0.65	17.50±0.38	26.70±0.48
8-9	-0.55±0.12	5.12±0.10	37.62±0.57	17.02±0.31	26.88±0.42
9-10	-0.29±0.21	4.75±0.17	36.31±0.92	15.56±0.43	26.70±0.68
10-12	-0.35±0.17	4.42±0.13	29.94±0.57	14.94±0.31	19.34±0.37
12-14	-0.76±0.28	4.38±0.19	19.32±0.59	14.62±0.45	10.18±0.30
14-16	-0.75±0.12	4.15±0.07	12.17±0.15	14.25±0.14	6.53±0.06
16-18	-0.96±0.12	4.12±0.07	10.89±0.14	14.19±0.14	4.98±0.05
18-20	-1.27±0.14	4.14±0.07	9.33±0.14	14.41±0.16	3.52±0.04
20-25	-0.93±0.08	3.60±0.04	6.17±0.06	13.35±0.09	2.01±0.01
25-30	-1.05±0.14	3.31±0.07	2.96±0.05	12.27±0.13	0.79±0.01
			Module 6		
4-5	-0.76±0.34	5.23±0.27	38.88±1.61	18.79±1.10	25.06±1.09
5-6	-0.83±0.27	5.33±0.22	40.29±1.34	18.94±0.90	25.65±0.92
6-7	-0.67±0.24	5.24±0.20	39.08±1.15	18.64±0.79	25.05±0.81
7-8	-0.62±0.14	5.04±0.11	38.98±0.67	17.28±0.36	26.64±0.46
8-9	-0.50±0.12	4.89±0.09	38.17±0.53	16.21±0.25	27.41±0.37
9-10	-0.39±0.22	4.62±0.17	39.53±0.98	15.28±0.39	27.98±0.67
10-12	-0.38±0.18	4.30±0.13	31.43±0.60	14.57±0.29	19.71±0.37
12-14	-0.60±0.26	4.17±0.17	18.94±0.54	14.12±0.40	10.14±0.28
14-16	-1.12±0.13	4.31±0.07	13.42±0.18	14.46±0.15	6.36±0.06
16-18	-1.37±0.13	4.32±0.07	11.72±0.17	14.64±0.16	4.62±0.05
18-20	-1.28±0.13	4.09±0.07	9.70±0.14	14.19±0.15	3.43±0.03
20-25	-1.56±0.10	3.87±0.05	6.80±0.09	13.95±0.11	1.85±0.01
25-30	-5.93±0.58	5.10±0.18	6.30±0.57	16.08±0.44	0.66±0.01
			Module 7		
4-5	-0.73±0.33	5.32±0.27	43.45±1.77	19.78±1.35	25.06±1.22
5-6	-0.92±0.28	5.46±0.22	44.90±1.52	20.00±1.12	25.46±1.02
6-7	-0.83±0.25	5.37±0.20	43.26±1.33	19.33±0.93	25.31±0.91
7-8	-0.77±0.15	5.17±0.12	40.93±0.74	17.35±0.39	26.39±0.50
8-9	-0.61±0.12	5.00±0.09	40.14±0.56	16.62±0.28	26.64±0.39
9-10	-0.56±0.22	4.78±0.17	40.19±1.02	15.70±0.44	25.98±0.67
10-12	-0.66±0.19	4.51±0.13	33.82±0.70	15.23±0.34	18.71±0.39
12-14	-0.77±0.27	4.20±0.17	19.67±0.57	14.31±0.40	9.68±0.26
14-16	-1.08±0.13	4.25±0.07	14.51±0.19	14.60±0.16	6.44±0.06
16-18	-1.29±0.13	4.22±0.07	12.66±0.18	14.70±0.16	4.66±0.05
18-20	-1.29±0.13	4.02±0.07	10.66±0.16	14.39±0.16	3.41±0.04
20-25	-1.47±0.09	3.72±0.04	7.36±0.09	13.60±0.10	1.91±0.01
25-30	-1.95±0.18	3.35±0.07	3.99±0.12	12.02±0.13	0.80±0.01
			Module 8		
4-5	-0.66±0.32	5.24±0.26	41.86±1.67	19.20±1.16	26.65±1.17
5-6	-0.93±0.27	5.49±0.22	42.05±1.43	20.12±1.11	25.09±0.98
6-7	-0.71±0.24	5.27±0.19	40.97±1.20	19.01±0.82	25.93±0.84
7-8	-0.63±0.15	5.07±0.12	39.28±0.69	17.20±0.36	27.55±0.48
8-9	-0.54±0.12	4.97±0.09	39.21±0.56	16.36±0.26	28.18±0.39
9-10	-0.41±0.20	4.76±0.16	38.45±0.92	15.65±0.42	26.07±0.64
10-12	-0.54±0.18	4.46±0.13	31.63±0.62	14.69±0.29	19.39±0.37
12-14	-1.09±0.31	4.49±0.19	19.14±0.64	14.44±0.45	9.50±0.29
14-16	-1.34±0.15	4.43±0.08	13.71±0.21	14.43±0.16	6.33±0.07
16-18	-1.69±0.16	4.40±0.08	12.02±0.21	14.48±0.17	4.61±0.05
18-20	-1.78±0.17	4.20±0.08	9.44±0.19	13.99±0.16	3.27±0.04
20-25	-2.27±0.14	4.20±0.06	6.61±0.12	14.44±0.13	1.57±0.01
25-30	-6.36±0.67	5.33±0.21	5.81±0.59	18.13±0.66	0.50±0.01

Table 5: $EA_E(\theta \equiv \theta_c)$ (cm^2)

Energy	Module 1	Module 2	Module 3	Module 4
4-5	66.74± 0.74	69.94± 0.79	66.61± 0.74	64.39± 0.69
5-6	67.81± 0.58	71.43± 0.62	64.77± 0.54	64.70± 0.52
6-7	67.42± 0.54	68.69± 0.56	66.89± 0.53	66.80± 0.52
7-8	68.49± 0.35	68.56± 0.36	66.79± 0.34	64.65± 0.31
8-9	69.88± 0.31	68.58± 0.31	67.34± 0.29	66.43± 0.27
9-10	69.57± 0.63	67.28± 0.60	64.35± 0.55	65.80± 0.56
10-12	53.14± 0.44	52.16± 0.44	51.87± 0.43	50.38± 0.40
12-14	31.55± 0.40	29.64± 0.37	30.80± 0.38	31.07± 0.38
14-16	21.95± 0.13	20.18± 0.12	20.04± 0.11	20.83± 0.12
16-18	17.83± 0.10	17.36± 0.10	16.29± 0.09	16.61± 0.10
18-20	13.84± 0.09	13.78± 0.09	12.67± 0.08	12.72± 0.08
20-25	9.49± 0.04	8.63± 0.04	8.31± 0.04	7.48± 0.04
25-30	4.69± 0.04	4.18± 0.03	3.62± 0.03	3.29± 0.03
Energy	Module 5	Module 6	Module 7	Module 8
4-5	62.94± 0.69	63.04± 0.72	67.72± 0.79	67.92± 0.77
5-6	64.30± 0.54	64.94± 0.57	69.33± 0.61	66.28± 0.56
6-7	62.73± 0.50	63.44± 0.53	67.67± 0.56	66.26± 0.53
7-8	63.42± 0.32	64.91± 0.33	66.58± 0.34	66.44± 0.34
8-9	64.11± 0.28	65.15± 0.29	66.27± 0.29	66.89± 0.29
9-10	62.91± 0.57	67.13± 0.64	65.71± 0.60	64.30± 0.56
10-12	49.06± 0.41	50.76± 0.44	51.65± 0.45	50.64± 0.41
12-14	29.13± 0.36	28.60± 0.37	28.60± 0.36	27.76± 0.33
14-16	18.21± 0.10	18.96± 0.11	20.04± 0.12	19.03± 0.11
16-18	15.21± 0.09	15.38± 0.09	16.29± 0.09	15.38± 0.09
18-20	12.10± 0.08	12.33± 0.08	13.15± 0.08	11.53± 0.08
20-25	7.76± 0.04	7.85± 0.04	8.44± 0.04	6.97± 0.03
25-30	3.48± 0.03	3.58± 0.03	3.98± 0.03	3.13± 0.03

Table 6: $HPD_E(\theta)$ (Eq. 4) fit parameters

Energy (keV)	θ_1 (arcmin)	σ_1 (arcmin)	A_1 (arcmin)	θ_2 (arcmin)	σ_2 (arcmin)	A_2 (arcmin)	A_3 (arcmin)
Module 1							
4-5	-9.91±0.49	7.25±0.35	-1.57±0.12	7.63±0.43	8.79±0.54	-1.77±0.15	2.35±0.16
5-6	-9.61±0.39	7.29±0.29	-1.60±0.10	7.86±0.36	8.66±0.42	-1.76±0.12	2.36±0.13
6-7	-10.16±0.33	7.72±0.25	-1.81±0.10	8.13±0.30	9.32±0.36	-2.04±0.12	2.68±0.13
7-8	-10.26±0.10	7.92±0.07	-1.85±0.03	8.40±0.09	9.46±0.11	-2.08±0.04	2.73±0.04
8-9	-10.30±0.08	7.78±0.06	-1.80±0.03	8.24±0.07	9.49±0.09	-2.05±0.03	2.68±0.03
9-10	-10.21±0.20	7.63±0.15	-1.71±0.06	8.06±0.18	9.43±0.23	-1.97±0.07	2.60±0.08
10-12	-9.46±0.19	7.09±0.15	-1.60±0.05	7.57±0.19	8.75±0.21	-1.83±0.06	2.45±0.07
12-14	-8.80±0.23	6.89±0.18	-1.69±0.06	7.31±0.23	8.10±0.23	-1.89±0.07	2.54±0.08
14-16	-8.74±0.22	5.99±0.15	-1.46±0.05	6.02±0.22	7.98±0.25	-1.82±0.06	2.40±0.06
16-18	-8.85±0.24	5.64±0.19	-1.35±0.06	5.37±0.27	8.28±0.30	-1.86±0.07	2.43±0.07
18-20	-8.38±0.33	5.74±0.25	-1.42±0.08	5.61±0.37	7.68±0.36	-1.83±0.08	2.41±0.09
20-25	-6.76±0.38	7.19±0.32	-1.63±0.07	7.68±0.37	6.31±0.26	-1.49±0.07	2.30±0.07
Module 2							
4-5	-6.55±0.38	8.42±0.46	-1.77±0.11	9.76±0.43	6.85±0.28	-1.49±0.09	2.33±0.12
5-6	-7.66±0.32	7.36±0.31	-1.60±0.09	8.63±0.38	7.63±0.27	-1.62±0.07	2.28±0.09
6-7	-7.57±0.25	7.69±0.24	-1.68±0.07	8.94±0.28	7.59±0.20	-1.66±0.06	2.37±0.07
7-8	-7.68±0.07	7.48±0.07	-1.63±0.02	8.79±0.09	7.71±0.06	-1.65±0.02	2.33±0.02
8-9	-7.72±0.06	7.55±0.07	-1.63±0.02	8.84±0.08	7.76±0.05	-1.65±0.01	2.33±0.02
9-10	-7.63±0.17	7.68±0.18	-1.62±0.05	8.86±0.21	7.75±0.14	-1.64±0.04	2.34±0.05
10-12	-7.35±0.15	6.88±0.15	-1.48±0.04	8.05±0.19	7.33±0.13	-1.54±0.03	2.18±0.04
12-14	-6.95±0.21	6.99±0.20	-1.71±0.06	8.02±0.24	7.02±0.16	-1.72±0.05	2.43±0.06
14-16	-6.79±0.22	6.42±0.19	-1.61±0.05	7.34±0.25	6.82±0.18	-1.68±0.04	2.36±0.05
16-18	-6.24±0.24	5.89±0.19	-1.53±0.05	6.82±0.26	6.26±0.19	-1.62±0.04	2.25±0.04
18-20	-6.81±0.32	5.47±0.24	-1.35±0.09	5.94±0.39	7.05±0.31	-1.70±0.06	2.28±0.06
20-25	-5.64±0.45	5.92±0.32	-1.34±0.09	6.87±0.51	6.34±0.31	-1.42±0.06	2.10±0.05
Module 3							
4-5	-9.70±0.49	7.99±0.44	-1.87±0.18	9.06±0.48	8.98±0.51	-2.01±0.19	2.65±0.22
5-6	-10.50±0.62	10.84±0.73	-3.64±0.54	11.95±0.69	10.09±0.60	-3.46±0.49	4.53±0.60
6-7	-10.22±0.31	8.16±0.27	-2.09±0.13	9.12±0.30	9.54±0.34	-2.31±0.15	2.97±0.16
7-8	-9.73±0.10	8.89±0.09	-2.31±0.05	10.05±0.09	9.05±0.10	-2.34±0.05	3.09±0.06
8-9	-9.76±0.09	8.83±0.08	-2.27±0.04	10.00±0.08	9.10±0.09	-2.31±0.04	3.04±0.05
9-10	-9.50±0.21	8.63±0.18	-2.12±0.09	9.80±0.19	8.84±0.21	-2.15±0.09	2.87±0.10
10-12	-8.74±0.21	8.07±0.18	-1.87±0.07	9.30±0.19	8.17±0.20	-1.88±0.08	2.59±0.09
12-14	-8.19±0.29	8.14±0.26	-2.03±0.10	9.29±0.28	7.95±0.26	-1.98±0.10	2.79±0.12
14-16	-8.13±0.33	7.50±0.25	-1.95±0.10	8.38±0.30	7.83±0.30	-2.01±0.11	2.79±0.12
16-18	-7.01±0.32	6.97±0.25	-1.66±0.07	7.92±0.28	6.66±0.27	-1.61±0.08	2.39±0.08
18-20	-5.99±0.41	6.95±0.37	-1.55±0.08	8.07±0.38	5.99±0.30	-1.41±0.09	2.23±0.10
20-25	-3.78±0.51	8.54±0.52	-1.45±0.07	9.11±0.29	5.06±0.33	-0.88±0.10	2.09±0.08
Module 4							
4-5	-6.83±0.37	8.81±0.47	-1.32±0.09	9.64±0.36	6.18±0.30	-1.06±0.07	1.86±0.10
5-6	-7.47±0.36	9.41±0.47	-1.58±0.12	10.14±0.37	6.78±0.30	-1.28±0.09	2.13±0.13
6-7	-7.65±0.27	9.28±0.34	-1.67±0.09	10.10±0.28	6.97±0.23	-1.38±0.07	2.25±0.10
7-8	-7.74±0.09	9.81±0.11	-1.74±0.03	10.51±0.09	7.16±0.08	-1.41±0.03	2.33±0.04
8-9	-7.71±0.08	9.90±0.09	-1.72±0.03	10.54±0.07	7.14±0.07	-1.38±0.02	2.30±0.03
9-10	-7.71±0.19	9.77±0.23	-1.68±0.07	10.42±0.18	7.09±0.16	-1.35±0.05	2.26±0.07
10-12	-7.52±0.20	9.05±0.22	-1.58±0.06	9.74±0.18	6.85±0.17	-1.31±0.05	2.18±0.06
12-14	-6.93±0.24	8.59±0.26	-1.55±0.06	9.20±0.21	6.41±0.19	-1.27±0.06	2.17±0.07
14-16	-7.44±0.34	9.27±0.38	-1.91±0.11	9.63±0.31	6.99±0.27	-1.55±0.10	2.59±0.13
16-18	-6.45±0.42	9.15±0.50	-1.79±0.12	9.47±0.38	6.46±0.31	-1.34±0.11	2.48±0.13
18-20	-6.36±0.54	6.84±0.44	-1.21±0.06	7.35±0.46	5.87±0.37	-1.11±0.08	1.94±0.07
20-25	-8.59±1.92	10.21±1.62	-2.10±0.55	10.45±1.85	9.32±1.53	-1.85±0.56	3.15±0.65

Table 7: $HPD_E(\theta)$ (Eq. 4) fit parameters *cont.*

Module 5							
4-5	-9.08±0.60	7.45±0.46	-1.72±0.16	7.95±0.58	8.56±0.60	-1.91±0.18	2.58±0.20
5-6	-8.57±0.55	8.09±0.47	-1.81±0.15	8.85±0.56	8.25±0.49	-1.81±0.16	2.56±0.18
6-7	-7.94±0.34	8.07±0.30	-1.73±0.08	8.81±0.32	7.45±0.28	-1.64±0.08	2.41±0.10
7-8	-8.35±0.11	8.12±0.09	-1.78±0.03	8.85±0.11	7.93±0.09	-1.74±0.03	2.52±0.03
8-9	-8.27±0.09	8.35±0.08	-1.82±0.03	9.11±0.09	7.93±0.08	-1.75±0.03	2.55±0.03
9-10	-8.26±0.24	8.32±0.21	-1.82±0.07	9.10±0.24	7.98±0.21	-1.75±0.07	2.56±0.08
10-12	-7.70±0.25	7.84±0.21	-1.69±0.06	8.64±0.24	7.49±0.20	-1.63±0.06	2.43±0.07
12-14	-6.76±0.31	7.92±0.28	-1.91±0.08	8.88±0.31	7.00±0.23	-1.71±0.08	2.63±0.09
14-16	-6.33±0.31	6.79±0.25	-1.65±0.06	7.77±0.31	6.49±0.23	-1.58±0.06	2.39±0.06
16-18	-6.84±0.42	6.68±0.31	-1.64±0.09	7.34±0.45	6.96±0.33	-1.68±0.08	2.47±0.08
18-20	-4.61±0.53	8.08±0.53	-1.83±0.11	9.04±0.48	5.78±0.35	-1.28±0.11	2.45±0.11
20-25	-3.92±0.44	9.51±0.59	-1.98±0.13	10.49±0.42	5.77±0.35	-1.11±0.11	2.56±0.14
Module 6							
4-5	-18.53±9.78	13.50±6.37	-6.94±10.60	13.18±5.47	21.04±12.61	-11.14±19.40	12.45±20.48
5-6	-17.30±3.16	14.32±2.79	-8.56±5.18	14.47±2.87	17.69±3.47	-10.48±6.29	12.22±7.04
6-7	-11.86±0.90	13.19±1.19	-5.06±1.18	14.10±1.16	12.10±0.88	-4.64±1.00	6.34±1.32
7-8	-13.47±0.30	12.81±0.34	-5.20±0.36	13.50±0.36	13.56±0.31	-5.45±0.35	6.92±0.42
8-9	-14.44±0.31	13.06±0.32	-5.67±0.38	13.59±0.35	14.61±0.32	-6.27±0.40	7.74±0.47
9-10	-13.29±0.68	12.87±0.81	-5.09±0.83	13.64±0.86	13.53±0.69	-5.29±0.79	6.78±0.97
10-12	-11.69±0.59	12.29±0.78	-4.38±0.64	13.16±0.81	12.04±0.57	-4.25±0.55	5.74±0.72
12-14	-10.59±0.63	10.55±0.68	-3.22±0.44	11.29±0.77	11.01±0.61	-3.31±0.40	4.52±0.50
14-16	-10.08±0.70	10.41±0.81	-3.35±0.54	11.41±0.95	10.86±0.67	-3.42±0.47	4.71±0.60
16-18	-6.75±0.51	10.28±0.79	-2.39±0.27	11.21±0.68	7.85±0.40	-1.78±0.17	3.21±0.28
18-20	-5.91±0.77	12.23±1.62	-3.18±0.66	13.02±1.13	8.09±0.66	-1.93±0.32	3.98±0.68
20-25	-1.19±0.20	90.62±7.71	-63.69±10.51	11.70±0.27	3.33±0.29	-0.44±0.04	64.31±10.51
Module 7							
4-5	-9.74±0.73	8.18±0.66	-1.89±0.27	9.00±0.76	9.14±0.75	-2.01±0.28	2.76±0.32
5-6	-10.17±0.70	8.38±0.60	-1.91±0.25	8.99±0.70	9.53±0.73	-2.08±0.28	2.84±0.31
6-7	-10.27±0.44	7.85±0.37	-1.82±0.16	8.47±0.43	9.75±0.50	-2.14±0.18	2.84±0.20
7-8	-10.14±0.16	8.21±0.12	-1.84±0.05	8.87±0.14	9.56±0.18	-2.06±0.06	2.80±0.07
8-9	-10.30±0.14	8.20±0.10	-1.84±0.04	8.85±0.11	9.74±0.15	-2.09±0.06	2.82±0.06
9-10	-10.57±0.36	8.12±0.25	-1.82±0.11	8.64±0.30	10.11±0.42	-2.15±0.15	2.88±0.16
10-12	-9.09±0.36	7.98±0.26	-1.73±0.09	8.64±0.31	8.53±0.35	-1.83±0.11	2.61±0.12
12-14	-8.50±0.42	7.35±0.28	-1.73±0.09	7.68±0.36	7.91±0.38	-1.85±0.12	2.65±0.12
14-16	-7.80±0.50	7.73±0.36	-1.99±0.12	8.11±0.44	7.51±0.40	-1.96±0.14	2.90±0.15
16-18	-7.49±0.48	6.73±0.31	-1.62±0.08	6.96±0.41	6.86±0.38	-1.70±0.11	2.50±0.10
18-20	-8.68±0.62	6.51±0.37	-1.68±0.13	6.26±0.53	7.81±0.61	-2.03±0.17	2.75±0.17
20-25	-9.12±0.67	6.72±0.44	-1.57±0.17	6.39±0.64	8.93±0.78	-2.09±0.22	2.83±0.22
Module 8							
4-5	-8.97±1.05	10.94±1.32	-2.83±0.60	11.47±1.25	9.23±0.87	-2.43±0.47	3.69±0.66
5-6	-9.15±0.69	9.34±0.65	-2.32±0.27	9.78±0.68	8.69±0.58	-2.23±0.26	3.16±0.31
6-7	-9.22±0.41	7.78±0.34	-1.65±0.11	8.12±0.43	8.69±0.38	-1.84±0.11	2.56±0.13
7-8	-8.53±0.11	8.20±0.10	-1.71±0.03	8.73±0.12	8.05±0.09	-1.72±0.03	2.53±0.03
8-9	-8.75±0.11	8.39±0.10	-1.77±0.03	8.88±0.11	8.31±0.09	-1.79±0.03	2.61±0.03
9-10	-8.79±0.28	8.39±0.25	-1.75±0.08	8.81±0.28	8.36±0.23	-1.78±0.07	2.60±0.09
10-12	-8.37±0.27	7.96±0.23	-1.64±0.06	8.29±0.27	7.84±0.22	-1.67±0.06	2.49±0.07
12-14	-7.91±0.33	7.63±0.27	-1.72±0.08	7.94±0.33	7.51±0.25	-1.75±0.07	2.59±0.08
14-16	-7.02±0.30	6.47±0.23	-1.35±0.05	6.79±0.30	6.52±0.22	-1.41±0.05	2.19±0.05
16-18	-5.65±0.36	7.60±0.34	-1.64±0.06	8.02±0.31	5.80±0.22	-1.35±0.07	2.41±0.07
18-20	-6.77±0.50	5.74±0.33	-1.18±0.07	5.83±0.48	6.20±0.36	-1.34±0.06	2.10±0.06
20-25	-5.31±0.93	7.96±0.70	-1.28±0.09	7.82±0.69	6.06±0.44	-1.02±0.14	2.15±0.08

Table 8: $HPD_E(\theta \equiv 0)$ (arcminutes)

Energy	Module 1	Module 2	Module 3	Module 4
4-5	0.522±0.229	0.487±0.177	0.544±0.295	0.562±0.136
5-6	0.521±0.183	0.494±0.138	0.539±0.783	0.563±0.171
6-7	0.523±0.182	0.503±0.110	0.548±0.220	0.573±0.136
7-8	0.527±0.056	0.507±0.033	0.553±0.074	0.569±0.047
8-9	0.522±0.046	0.501±0.029	0.545±0.062	0.560±0.040
9-10	0.529±0.109	0.503±0.077	0.552±0.138	0.570±0.096
10-12	0.534±0.093	0.506±0.063	0.565±0.118	0.585±0.088
12-14	0.528±0.112	0.489±0.094	0.565±0.169	0.591±0.095
14-16	0.534±0.094	0.495±0.091	0.580±0.177	0.611±0.174
16-18	0.528±0.110	0.487±0.092	0.589±0.131	0.630±0.189
18-20	0.514±0.138	0.461±0.125	0.583±0.154	0.648±0.134
20-25	0.540±0.128	0.459±0.140	0.596±0.120	0.694±0.913
Energy	Module 5	Module 6	Module 7	Module 8
4-5	0.517±0.288	0.590±26.654	0.593±0.438	0.539±0.883
5-6	0.513±0.261	0.597±8.977	0.592±0.422	0.545±0.432
6-7	0.525±0.146	0.611±1.683	0.601±0.274	0.556±0.188
7-8	0.531±0.050	0.612±0.540	0.602±0.093	0.575±0.051
8-9	0.525±0.044	0.600±0.598	0.595±0.080	0.568±0.049
9-10	0.535±0.113	0.610±1.240	0.604±0.216	0.576±0.125
10-12	0.548±0.102	0.621±0.927	0.616±0.170	0.588±0.111
12-14	0.540±0.135	0.624±0.662	0.605±0.181	0.587±0.134
14-16	0.548±0.113	0.641±0.796	0.617±0.230	0.619±0.092
16-18	0.539±0.155	0.641±0.381	0.617±0.174	0.640±0.117
18-20	0.521±0.178	0.622±0.924	0.590±0.271	0.647±0.135
20-25	0.526±0.192	0.630±14.869	0.584±0.327	0.676±0.178

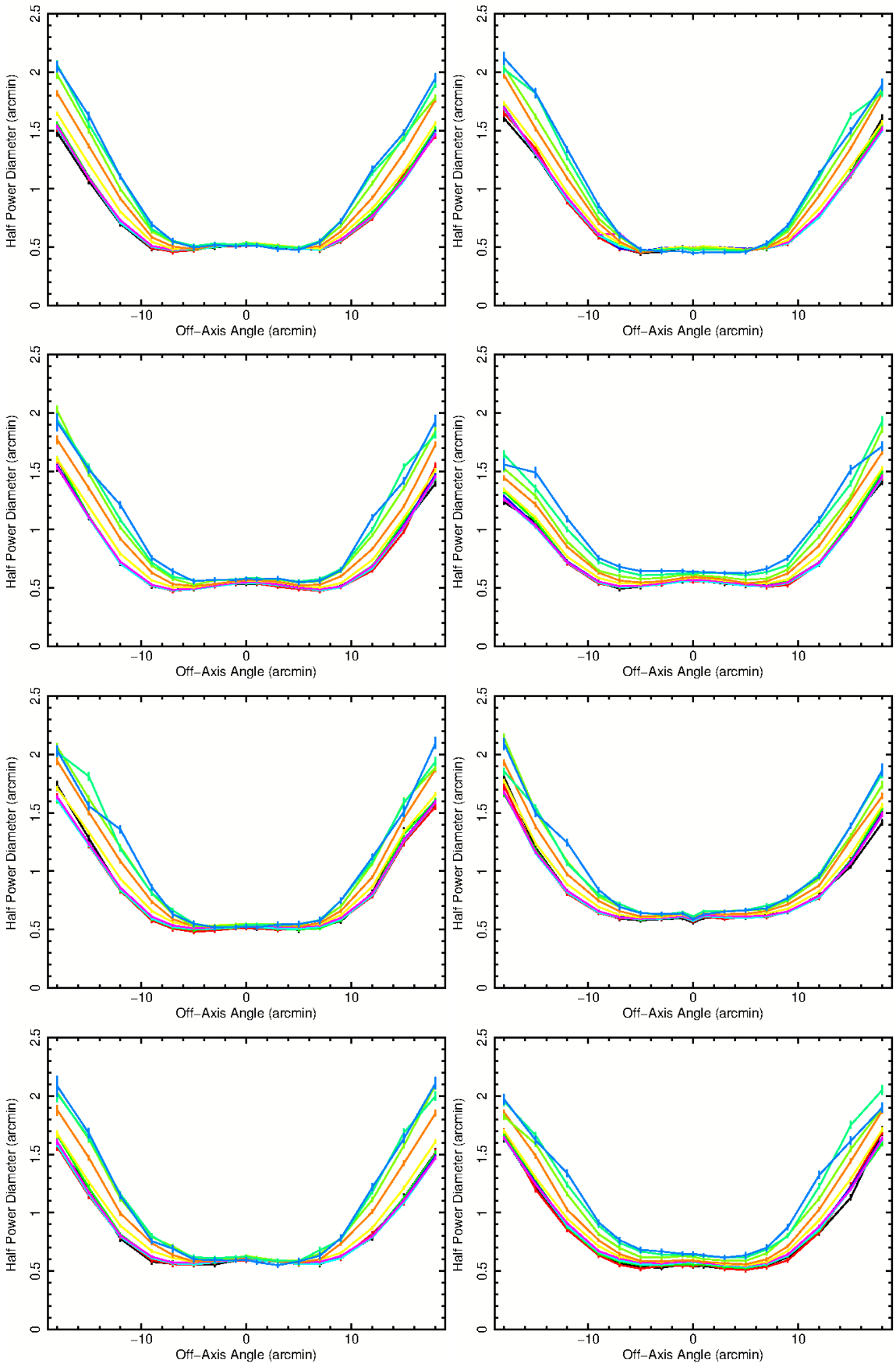

Figure 4: Half-power diameter, $HPD_E(\theta)$, against off-axis angle, θ. Each panel contains 11 curves for the first 11 energy groups, E_g, the uncertainties in the two highest energy groups are too large to meaningfully constrain the HPD. From left-to-right, top-to-bottom, the 8 modules are shown in order.